Supporting Information

Multifunctional Ti$_3$C$_2$ Decorated Perovskite La$_{1-x}$Sr$_x$CoO$_3$ Nanorods for Efficient Energy Conversion

Hao Zhang,[a] Yi Lu,*[a] Deqi Fan,[a] Xueling Xu,[a] Xiaodong Li [a], Xiaofei Yang*

[a] Jiangsu Co-Innovation Center of Efficient Processing and Utilization of Forest Resources, International Innovation Center for Forest Chemicals and Materials, College of Science, Nanjing Forestry University, Nanjing 210037, PR China

* Corresponding Author.

E-mail addresses: yilu@njfu.edu.cn (Y. Lu)

1. Experimental Section

1.1 Chemicals

Lanthanum nitrate hexahydrate (La(NO$_3$)$_3 \cdot$6H$_2$O, 99.99 wt%), cobalt-nitrate hexahydrate (Co(NO$_3$)$_2 \cdot$6H$_2$O, 99.99 wt%), potassium hydroxide (KOH, ≥90 wt%), ammonium fluoride (NH$_4$F, 95%) and isopropanol (C$_3$H$_8$O, >99.9 wt%) were purchased from Aladdin. Strontium nitrate (Sr(NO$_3$)$_2$, 99.5 wt%), hydrochloric acid (HCl, 36−38 wt%), and absolute ethanol (C$_2$H$_5$OH) were purchased from Sinopharm Chemical Reagent Co., Ltd. Conductive carbon black (C, super P), Nafion solution (5 wt%) and hexamethylenetetramine (C$_6$H$_{12}$N$_4$, ≥99 wt %) were purchased from Sigma−Aldrich. Titanium aluminum carbide (Ti$_3$AlC$_2$, 98 wt %) was obtained from Laizhou Kai Kai Ceramic Materials Co., Ltd. Deionized (DI) water (18.2 MΩ cm of resistivity) was purified using a RODI−220A1 purification system. Analytical reagent grade chemicals and solvents were utilized without additional purification.

1.2 Synthesis of MXene, perovskite oxide and composites

1.2.1 Preparation of MXene (Ti$_3$C$_2$)

In a typical experiment, the etched treatment and delamination of MXene flakes were prepared using a reported method in our previous works [1, 2]. Ti$_3$AlC$_2$ powder (0.5 g) was added to a Teflon−lined autoclave containing HCl (36−38 %, 20 mL) and NH$_4$F (95 %, 2.96 g). The mixture was maintained at 60 °C and stirred for 72 h at 600 rpm. After centrifuging at 3000 rpm for 10 min, the black slurry was transferred to a centrifuge tube (50 mL), followed by washing with deionized (DI) water for several

times until the pH reached 6. After that, the black slurry was freeze dried for 12 h to obtain Ti_3C_2 powders. Finally, dimethyl sulfoxide (DMSO) and Ti_3C_2 powders were mixed by stirring for 48 h at 500 rpm in N_2. The obtained powders were then freeze dried for 12 h after washing and centrifuging for several times.

1.2.2 Preparation of perovskite oxides and LSC1/MXene composite

The precursor solution for the LSC1 was prepared by dissolving $La(NO_3)_3 \cdot 6H_2O$ (0.9 mmol), $Co(NO_3)_2 \cdot 6H_2O$ (1 mmol), $Sr(NO_3)_2$ (0.1 mmol), and hexamethylenetetramine (HMTA, 2 mmol) in deionized water (20 mL) and Methyl alcohol (MT, 20 mL). The La−Sr−Co precursor was heated at $200^{\circ}C$ for 48 h. Furthermore, the La−Sr−Co hybrid composite was high−speed centrifugated and rinsed with anhydrous ethanol and deionized water several times before being freeze−dried for 12 h. Subsequently, the obtained La−Sr−Co hybrid composite was thermally treated at 900, 1000 and $1100^{\circ}C$ for 3 h in N_2 with a rate of $5^{\circ}C$ min^{-1}, which were named as LSC1−900, LSC1−1000, and LSC1−1100. Meanwhile, the LC0, LSC1, LSC3, LSC5, LSC7 and LSC9 were prepared using the same method by controlling the mole ratio of Co to La and Sr (1:1:0, 1:0.9:0.1, 1:0.7:0.3, 1:0.5:0.5, 1:0.3:0.7 and 1:0.1:0.9). Subsequently, the La–Sr–Co perovskite oxides were calcinated at 500, 600, and 700 $^{\circ}C$ for 3 h in N_2 at 5 $^{\circ}C$ min^{-1}. For comparison, the LSC1 was prepared using the same method, except that the pH of precursor solution was adjusted to 10, 11, 12 and 13. In addition, the LSC1/MXene (LSM) was synthesized using the same method as that of LSC1, with the exception that MXene (50 mg) was added to the precursor solution. The

LSC1+MXene powder (m_{LSC1}: m_{MXene}= 5: 1) was obtained by simple physical mixing LSC1 and MXene method.

1.2.3 Preparation of photothermal films

The membranes were prepared by a simple vacuum-assisted titration method using different photothermal materials. Taking LSC1 membrane as an example, The LSC1 powder (30 mg) was dispersed in DI water (10 mL), and then was vacuum−filtered to a membrane using a polypropylene membrane (3501 Coated PP, Celgard LLC, Charlotte, NC).

1.3 Material Characterization

X-ray diffraction (XRD, Ultima IV, Rigaku, Japan) was conducted by utilizing Cu K radiation with a step size of 10° and a dwell period of 1 min, in the 2θ range of 5°~ 80°. The morphology and flake microstructure of the acquired samples were examined using a scanning electron microscope (SEM, JSM−7600 F, JEOL, Japan). The X-ray photoelectron spectroscopy (XPS) examination was performed on an ESCALAB 250Xi X-ray photoelectron spectrometer (Thermo Scientific, USA), and the data from the samples was fitted using the software program XPS PEAK. An ASAP 2020 Analyzer was used to analyze the specific surface area (BET) and pore size distribution of the samples (Micromeritics Instruments, USA). The N_2 sorption isotherms were obtained at 77 K.

1.4 Electrochemical measurement

Electrochemical studies were carried out in 1.0 mol L^{-1} KOH solution at room temperature using a CHI 760E electrochemical analytical equipment with a three−electrode system. To prepare the working electrode, the catalyst powder was mixed with conductive carbon black and ethanol/isopropanol/Nafion (1 ‰ Nafion) solution in a weight ratio of 2:1:160, and ultrasonically dispersed for 15 min to prepare a homogeneous ink. 20 µL of the catalyst dispersion was then coated on a glassy carbon electrode with 0.196 cm^2 area and dried at room temperature for electrocatalysis test. The saturated Ag/AgCl electrode as the reference electrode, and the graphite rod was used as the counter electrode. The Linear sweep voltammetry (LSV) and cyclic voltammetry (CV) curves were measured with the scan rate of 5 mV s^{-1} in 1.0 mol L^{-1} KOH aqueous solution. All measured potential results were corrected to potential relative to reversible hydrogen electrode (RHE) based on Nermst equation for comparison, and the following formula might be used to convert RHE and saturated silver chloride electrode potential:[1]

$$E_{(vs.\ RHE)} = E_{(vs.\ Ag/AgCl)} + 0.059 \times pH + 0.197\ V \tag{1}$$

Where $E_{(vs.\ RHE)}$ is the corrected reversible hydrogen electrode potential, $E_{(vs.\ Ag/AgCl)}$ is the measured actual potential, 0.197 V is the standard electrode potential of the reference electrode, and pH = 13.85. Amperomatric i-t curve (i-t) was used to study the long−term durability of the catalyst in 1.0 mol L^{-1} KOH aqueous solution for 10 h cycles using a rotating disk electrode (RDE). Electrochemical

impedance spectroscopy (EIS) experiments were carried out in the frequency range of 0.001 to 100 kHz in the laboratory. The synthesis method of the ink used in EIS test was similar to the above method, except that conductive carbon black was not added in the Nafion solution.

1.5 Characterization of solar absorption performance

The UV-vis-NIR spectrometer (UVPC, Lambda 950, PE) was used to measure the optical diffuse reflection properties of the samples at wavelengths ranging from 250 nm to 2500 nm. The following formula can be used to determine the solar absorptivity (α) of samples:[2]

$$\alpha = 1 - R(\lambda) - T(\lambda) = \frac{\int_{250}^{2500} I(\lambda)(1 - R(\lambda))d\lambda}{\int_{250}^{2500} I(\lambda)d\lambda}$$

(2)

Where $I(\lambda)$ is the light intensity function of the sun spectrum at various wavelengths, $T(\lambda)$ is 0 since the sample is opaque, and $R(\lambda)$ is the reflectance of the samples at different wavelengths (λ).

1.6 Photothermal performance

The solar evaporation experiments were carried out in the laboratory to determine the average solar thermal conversion capability. A solar simulator (CEAULIGHT's CEL−PE300L−3A, China) and an AM1.5 optical filter was utilized to provide simulated sunlight. An optical power meter was used to measure the simulated sunshine intensity (CEL−NP2000−2, CEAULIGHT, China). Water loss was measured using a high−precision electronic balance that was linked to a computer. A thermal imager

6

(FLIR, E8) was used to monitor and record the temperature change of the samples' surface during photothermal evaporation process. The surrounding conditions were kept at 35 ± 5% relative humidity and 25 ± 0.5 °C ambient temperature.

2. Heat loss analysis

During solar evaporation, the heat loss includes thermal convection, conduction and radiation. The calculated equations are as follows.

Convective heat loss $\qquad Q_{convective} = A_s h(T_0 - T_1)$ $\qquad\qquad$ (1)

Thermal radiation loss $\qquad Q_{radiation} = A_s \varepsilon \sigma(T_0^4 - T_1^4)$ $\qquad\qquad$ (2)

Thermal conduction loss $\qquad Q_{radiation} = Cm\Delta T$ $\qquad\qquad$ (3)

Where A_s is the irradiation area (≈ 13 cm^2), h is the convection heat transfer coefficient (5 W m^{-2} K), ε represents the emissivity of the object (≈ 0.85), σ is the Stefan-Boltzmann constant (5.67×10^{-8} W m^{-2} K^{-4}), C is the specific heat capacity of water (4200 J/°C kg), m is the weight of water, ΔT (0.1 °C) is the average temperature change of the bottom water after 1 h illumination, T_0 is the average surface temperature of the LSM (38.1°C), T_1 is the ambient temperature of the surrounding fluid (35.8°C).

Accordingly, the thermal radiation loss, thermal convection loss, and thermal conduction loss were calculated to be 1.27%, 1.42%, and 0.49%, which matched well with the deficiency of energy convesion efficiency (~96.8%).
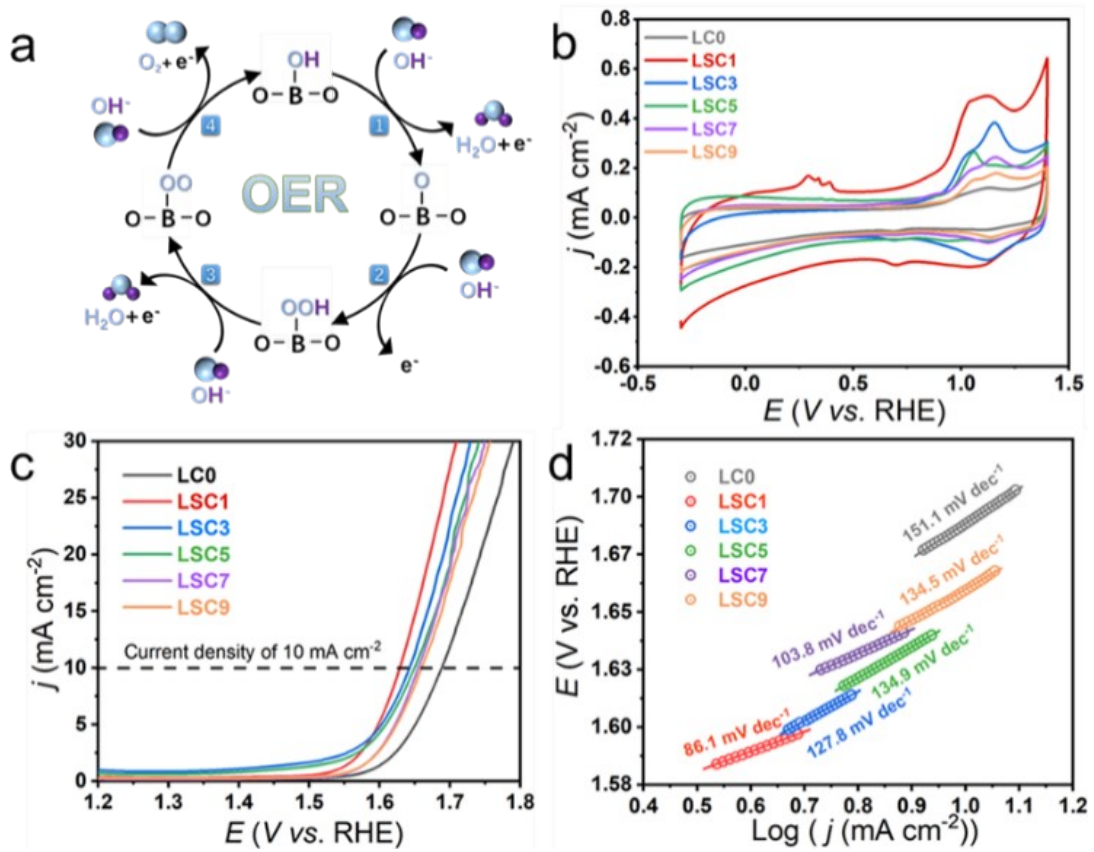
Fig. S1 The OER performance of the $La_{1-x}Sr_xCoO_3$ in 1 M KOH. (a) Schematic illustration of OER mechanism of perovskite oxides in 1 M KOH. (b) CV curves, (c, d) The LSV curves and corresponding Tafel plots of $La_{1-x}Sr_xCoO_3$ in 1 M KOH. Scan rate, 5 mV s^{-1}.
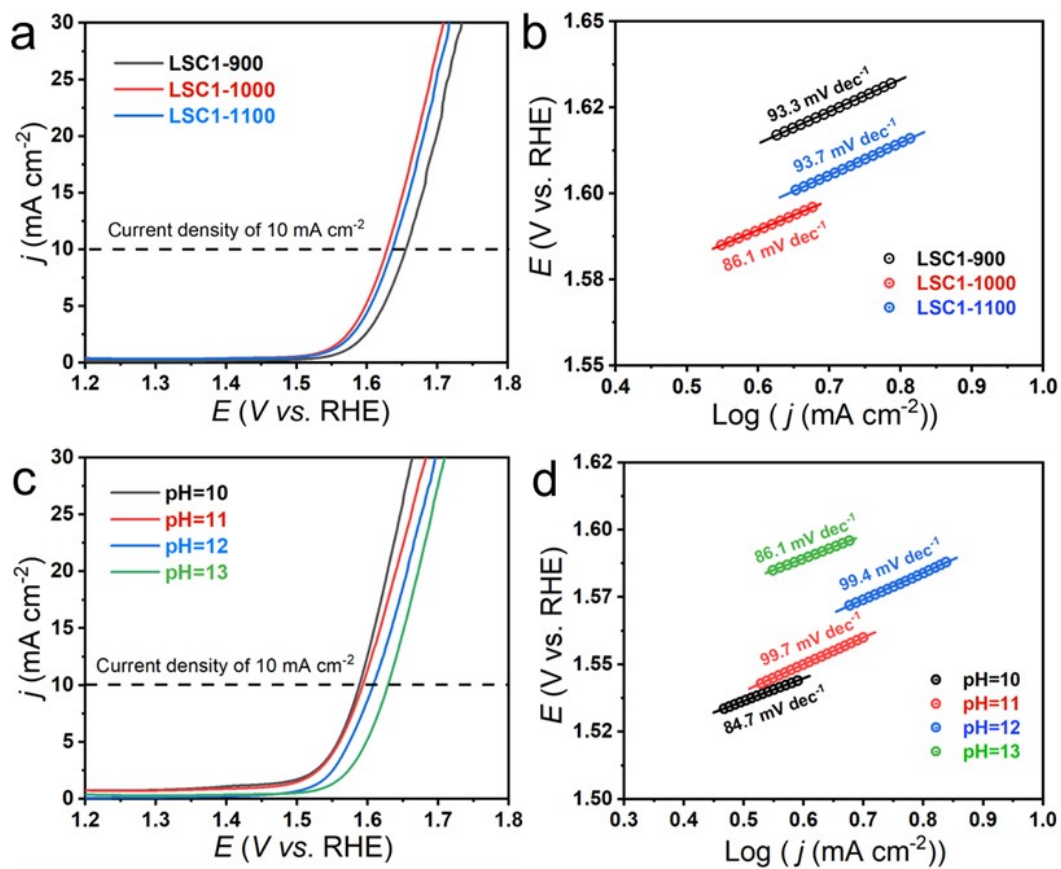
Fig. S2 The OER performance of the $La_{0.9}Sr_{0.1}CoO_3$ prepared at various conditions. (a, b) The LSV curves and corresponding Tafel plots of LSC1-900, LSC1-1000 and LSC1-1100 in 1 M KOH. Scan rate, 5 mV s^{-1}. (c, d) The LSV curves and corresponding Tafel plots of the composites prepared at different pH solutions. Scan rate, 5 mV s^{-1}.
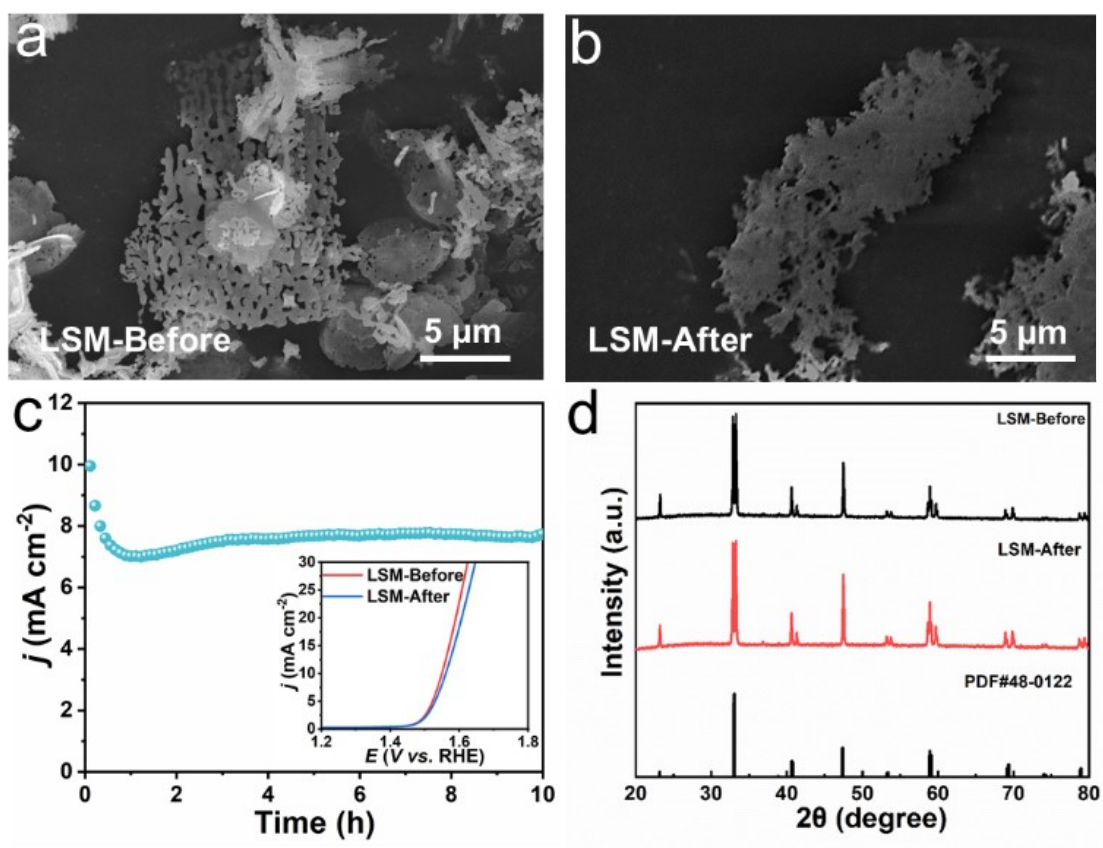
Fig. S3 Structural characterization of LSM before and after long-term electrocatalysis. (a, b) SEM images of LSM−Before and LSM−After. (c) The of OER performance stability of the LSM in 1 M KOH. (d) X-ray diffraction patterns of LSM−Before and LSM−After.
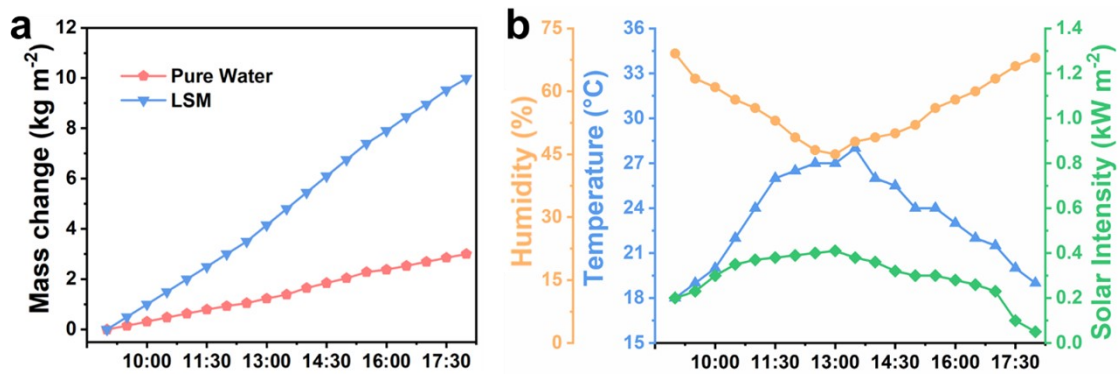
Fig. S4 (a) Mass change of photothermal evaporator in outdoor experiment. (b) Solar intensity, temperature and humidity during the outdoor experiment.

Table S1. Comparison of evaporation performance with solar photothermal evaporators in recent literature reports.

Materials	Structure	Evaporation Rate (kg m^{-2} h^{-1})	Energy efficiency (%)	Reference
MXene/CIS	photothermal membrane	1.43	90.04	[3]
MXene/PDA	3D carbon networks	1.598	89.9	[4]
polyimide/MXene	3D aerogel	14.4 (4 sun)	81	[5]
Xylem-Inspired polyimide/MXene	3D aerogel	2.09	94.4	[6]
Chitosan/MXene/ fabric	3D fabric architectures	1.58	88.05	[7]
PDA/PEI@PVDF -HFP@MXene	sandwich-structured nanofibrous membrane	3.782 (3 sun)	95.45	[8]
rGO/MXene-PPS	fibrous membrane	1.235	97	[9]
MXene/CNT	photothermal membrane	1.66	99.73	[10]
MXene/Tissue	3D composite film	1.85	90	[11]
MXene/MMT	self-assembly hierarchical binary gel	1.37	93.7	[12]
La$_{0.9}$Sr$_{0.1}$CoO$_3$/Ti$_3$C$_2$ MXene	**photothermal membrane**	**1.40**	**96.8**	**This work**

References

[1]   Y. Lu, D. Q. Fan, Z. P. Chen, W. P. Xiao, C. C. Cao and X. F. Yang, *Sci. Bull.*, 2020, **65**, 460-466.

[2]   D. Q. Fan, Y. Lu, H. Zhang, H. L. Xu, C. H. Lu, Y. C. Tang and X. F. Yang, *Appl. Catal. B Environ.*, 2021, **295**, 120285.

[3]   Y. Wang, J. Nie, Z. He, Y. Zhi, X. Ma and P. Zhong, *ACS Appl. Mater. Interfaces*, 2022, **14**, 5876-5886.

[4]   Y. Jin, K. Wang, S. Li and J. Liu, *J. Colloid Interface Sci.*, 2022, **614**, 345-354.

[5]   L. Pu, H. Ma, J. Dong, C. Zhang, F. Lai, G. He, P. Ma, W. Dong, Y. Huang and T. Liu, *Nano Lett.*, 2022, **22**, 4560-4568.

[6]   Z. Zheng, W. Li, H. Liu and X. Wang, *ACS Appl. Mater. Interfaces*, 2022, **14**, 50966-50981.

[7]   Z. Wu, J. Li, S. Zhang, J. Yan, J. Gao, N. Zheng and H. Xue, *J. Colloid Interface Sci.*, 2022, **622**, 169-180.

[8]   H. Bai, T. Fan, H. Guan, Y. Su, J. Zhang, J. Wang, S. Ramakrishna and Y.Z. Long, *Compos. Commun.*, 2022, **31**, 101104.

[9]   G. Wang, J. Miao, X. Ma, C.W. Lou, J.H. Lin, Y.Z. Long, S. Ramakrishna and T. Fan, *Sep. Purif. Technol.*, 2022, **302**, 122014.

[10]   Y. Shang, B. Li, C. Xu, R. Zhang and Y. Wang, *Sep. Purif. Technol.*, 2022, **298**, 121597.

[11]   R. Ding, H. Zheng, X. Zhao, F. Xue, P. Li, J. Xiong, Z. Chen, Z. Liu, Q. Peng and X. He, *Compos. Part A-Appl. S.*, 2022, **158**, 106967.

[12]   Z. Ai, Y. Zhao, R. Gao, L. Chen, T. Wen, W. Wang, T. Zhang, W. Ge and S. Song, *J. Clean. Prod.*, 2022, **357**, 132000.